Kinetic Analyses of Mutations in the Glycine-Rich Loop of cAMP-Dependent Protein Kinase†

Bruce D. Grant,‡ Wolfram Hemmer,‡,§ Igor Tsigelny,‡ Joseph A. Adams,|| and Susan S. Taylor*,‡

Howard Hughes Medical Institute, Department of Chemistry and Biochemistry, University of California at San Diego, 9500 Gilman Drive, La Jolla, California 92093-0654, and Department of Chemistry, San Diego State University, San Diego, California 92182-1030

Received December 4, 1997; Revised Manuscript Received March 19, 1998

ABSTRACT: The conserved glycines in the glycine-rich loop (Leu-Gly$_{50}$-Thr-Gly$_{52}$-Ser-Phe-Gly$_{55}$-Arg-Val) of the catalytic (C) subunit of cAMP-dependent protein kinase were each mutated to Ser (G50S, G52S, and G55S). The effects of these mutations were assessed here using both steady-state and pre-steady-state kinetic methods. While G50S and G52S reduced the apparent affinity for ATP by approximately 10-fold, substitution at Gly55 had no effect on nucleotide binding. In contrast to ATP, only mutation at position 50 interfered with ADP binding. These three mutations lowered the rate of phosphoryl transfer by 7−300-fold. The combined data indicate that G50 and G52 are the most critical residues in the loop for catalysis, with replacement at position 52 being the most extreme owing to a larger decrease in the rate of phosphoryl transfer (29 vs 1.6 s^{-1} in contrast to 500 s^{-1} for wild-type C). Surprisingly, all three mutations lowered the affinity for Kemptide by approximately 10-fold, although none of the loop glycines makes direct contact with the substrate. The inability to correlate the rate constant for net product release with the dissociation constant for ADP implies that other steps may limit the decomposition of the ternary product complex. The observations that G52S (a) selectively affects ATP binding and (b) significantly lowers the rate of phosphoryl transfer without making direct contact with either the nucleotide or the peptide imply that this residue serves a structural role in the loop, most likely by positioning the backbone amide of Ser53 for contacting the γ-phosphate of ATP. Energy-minimized models of the mutant proteins are consistent with the observed kinetic consequences of each mutation. The models predict that only mutation of Gly52 will interfere with the observed hydrogen bonding between the backbone and ATP.

Many nucleotide binding enzymes utilize glycine-rich loops that help position nucleotides for catalysis (*1*−*3*). Crystal structures of dinucleotide and mononucleotide binding enzymes define several glycine-rich loops that are distinct both in their amino acid sequence and in their orientation relative to the nucleotide. The glycine-rich loops found in dinucleotide binding enzymes [e.g., pyruvate dehydrogenase (*4*) and dihydrofolate reductase (*5*)] are typically Gly-X-Gly-X-X-Gly and provide space for the dinucleotide pyrophosphate moiety. The glycine-rich loops, or P-loops, found in mononucleotide binding enzymes [e.g., p21ras (*6*), adenylate kinase (*7*), Rec A (*8*), and elongation factor Tu (*9*)] have the consensus sequence Gly-X-X-X-X-Gly-Lys-Ser/Thr and interact with the γ-phosphate of ATP (*10*). In contrast, the protein kinase family of enzymes contain a glycine-rich loop with a consensus sequence Gly-X-Gly-X-X-Gly-X-Val. On the basis of numerous crystal structures, this loop is part of a β-hairpin that connects β-strands 1 and 2 and serves as a nucleotide-positioning loop (NPL)[1] that interacts with all three phosphates of ATP (*11*−*15*). The glycines in the protein kinase NPL are highly conserved; the first, second, and third glycines are conserved in 95, 100, and 85% of protein kinases, respectively (*16*).

The catalytic subunit (C-subunit) of cAMP-dependent protein kinase (cAPK) regulates many processes, including glycogen metabolism and neurotransmitter activity (*17*), and also modulates mitogenic signal transduction through the Ras-mitogen activated protein kinase pathway (*18*) in response to the second messenger, cAMP (*19*). The C-subunit catalyzes transfer of the γ-phosphate from ATP to Ser and Thr hydroxyls in protein substrates. The enzyme−MgATP−IP_{20} ternary complex crystal structure of the C-subunit (*20*) consists of an N-terminal lobe that is mostly β-structure and a larger C-terminal lobe that is primarily α-helix. MgATP and substrate bind to the enzyme's active site which is formed at the junction of these two lobes, and

† This work was supported by NIH Grant GM19301 to S.S.T., NIH Training Grant T32GM07313 to B.D.G., and NIH Grant GM54846 to J.A.A.

* To whom correspondence should be addressed. Phone: (619) 534-5554. Fax: (619) 534-8193. E-mail: staylor@ucsd.edu.

‡ University of California at San Diego.

§ Current address: Division of Food Science, Swiss Federal Office of Public Health, CH-3003 Bern, Switzerland.

|| San Diego State University.

[1] Abbreviations: AMPPNP, adenylyl imidodiphosphate; cAMP, cyclic nucleotide monophosphate; DTT, dithiothreitol; Mops, 3-(*N*-morpholino)propanesulfonic acid; cAPK, cAMP-dependent protein kinase; C-subunit, catalytic subunit; LRRASLG, Kemptide; LRRAS-(P)LG, phospho-Kemptide; NPL, nucleotide-positioning loop; IP_{20}, heat stable 20-amino acid protein kinase inhibitor peptide.

S0006-2960(97)02987-5 CCC: $15.00
Published on Web 05/02/1998

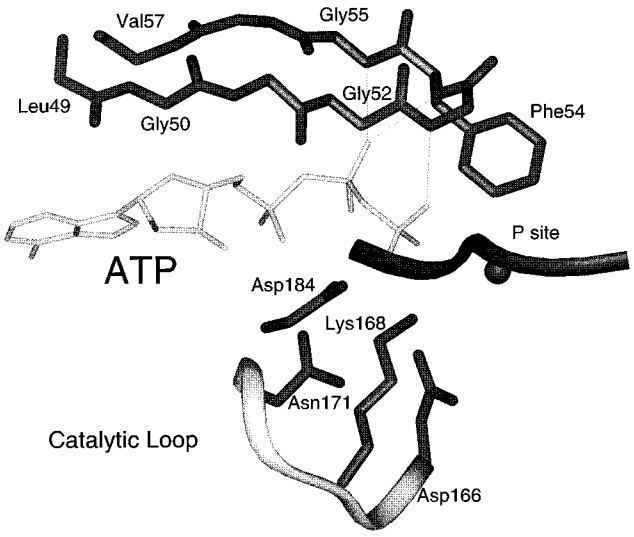

FIGURE 1: C-Subunit active site with bound nucleotide. The glycine-rich loop clamps the nucleotide into position with Gly50 over the ribose, Gly52 above the γ-phosphate, and Gly55 near the β-phosphate. The nucleotide γ-phosphate is also within hydrogen bonding distance of the ϵ-amino moiety of Lys168, and magnesium ions coordinated by invariant residues, Asp184 in the magnesium-positioning loop, and Gln171 in the catalytic loop. The putative catalytic base, Asp166, also in the catalytic loop, is close to the hydroxyl moiety of the P site residue that in a substrate accepts the phosphate. The catalytic loop (residues 166−171) and the P−3 to P1 position of the inhibitor peptide are indicated as ribbons. The P site Ala is indicated by a ball. In a substrate peptide, this would be a Ser or Thr. Hydrogen bonds between the glycine-rich loop and the nucleotide are indicated with dashed lines.

the NPL (Leu_{49}-Gly-Thr-Gly-Ser-Phe-Gly-Arg-Val_{57}), located in the small lobe, forms the active site ceiling (Figure 1). This sequence, which is well-ordered only in the C−ATP−IP_{20} ternary complex, interacts with several parts of ATP in the following manner: (i) the Leu49 and Val57 side chains form hydrophobic contacts with the nucleotide adenine moiety, (ii) the Gly50 backbone amide forms a hydrogen bond with the ribose, (iii) the Ser53 backbone amide interacts with the axial oxygen of the ATP γ-phosphate, and (iv) the Gly55 backbone amide forms a hydrogen bond with the axial oxygen of the ATP β-phosphate (*14*, *20*, *21*). Amino acids from the large lobe that form the floor of the active site are also illustrated in Figure 1. The Lys168 ϵ-amino group forms an electrostatic interaction with the ATP γ-phosphoryl oxygen, and the Asp184 carboxylate coordinates a magnesium ion which, in turn, coordinates with both the β- and γ-phosphate oxygens. Asp166 forms a hydrogen bond with the substrate's hydroxyl, the phosphoryl acceptor, and may serve as a weak general base catalyst (*22*).

Although purifications and perturbations in steady-state kinetic parameters were described previously for mutants of the glycine-rich loop of the C-subunit, the exact effects of these mutations on individual steps in the reaction mechanism were not reported (*23*). The general effects of mutations in the glycine-rich loop of the phosphorylase kinase γ-subunit were also described previously (*24*).

In this report, kinetic parameters for three cAPK C-subunit mutants, Gly50 to Ser (G50S), Gly52 to Ser (G52S), and Gly55 to Ser (G55S), were measured on the steady-state and pre-steady-state kinetic time frames. Without the pre-steady-state kinetics, the full impact of the mutations is not fully appreciated. A comparison of the mutant proteins to the wild-type C-subunit defines the contribution of the glycine triad to ternary complex formation, phosphoryl transfer, and net product release in the kinetic reaction pathway. The data are interpreted according to the wild-type kinetic mechanism. This mechanism, shown in Scheme 1, is derived from a combination of rapid quench flow and viscosometric studies (*25*, *26*).

Although the reaction scheme is random, the initial binding of ATP is preferred followed by the substrate (Kemptide) on the basis of thermodynamic reasons (*27*, *28*). The substrate is in rapid exchange with the enzyme, while ATP is catalytically committed (i.e., $k_3 > k_{-1}$). The ternary complex supports a rapid phosphoryl transfer step (k_3), and the rate-determining step in turnover is the net release of products (k_4). For wild-type cAPK, the last step is controlled by ADP dissociation (*22*).

EXPERIMENTAL PROCEDURES

Materials. Adenosine triphosphate (ATP), adenosine diphosphate (ADP), cyclic adenosine monophosphate (cAMP), 5′-adenylyl imidodiphosphate (AMPPNP), 3-(*N*-morpholino)-propanesulfonic acid (Mops), dithiothreitol (DTT), lactate dehydrogenase, pyruvate kinase, reduced nicotinamide adenine dinucleotide (NADH), and phosphoenolpyruvate were purchased from Sigma Chemicals. Isopropyl β-D-thiogalactopyranoside (IPTG) was purchased from United States Biochemical. Magnesium chloride, phosphoric acid, β-mercaptoethanol, and liquid scintillant were purchased from Fisher Scientific. Phosphocellulose filter disks were purchased from Whatman. Ni^{2+}−agarose was purchased from Qiagen, and [γ-^{32}P]ATP and [α-^{35}S]dATP were purchased from ICN Laboratories. The heptameric peptides, LRRASLG (Kemptide) and LRRAALG, were synthesized at the Peptide and Oligonucleotide Facility at the University of California, San Diego, and purified by high-performance liquid chromatography after synthesis.

Mutagenesis, Expression, and Purification of C-Subunits. Glycine mutations were introduced into the mouse C-subunit gene by an oligonucleotide-directed method (*23*). Transformed bacteria were cultured in YT media containing 200 μg/mL ampicillin, and gene expression was induced with 1 mM IPTG once the culture's optical density was 0.6 AU at 600 nm. At the end of a 5 h induction, cells were harvested by centrifugation at 4000*g* for 10 min. Wild-type C-subunit was purified as described previously (*29*). C-Subunit mutants were complexed with a polyhistidine-tagged regula-

Scheme 1

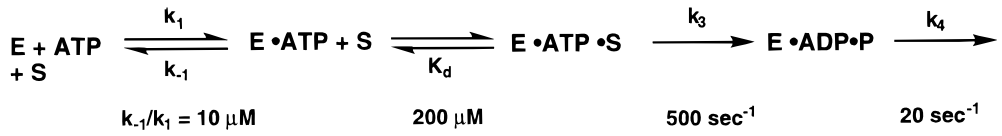

tory subunit type II mutant, adsorbed to Ni^{2+}−agarose, and eluted from the holoenzyme complex with 1 mM cAMP (*30*). Mutants were further resolved on the basis of differing phosphorylation states by chromatography on Mono S FPLC (*29*). For these studies, isoforms II and III were used which correspond to the enzyme that is phosphorylated at Ser10, Thr197, and Ser339 (isoform II) and Ser338 and Thr197 (isoform III) (*23*). Pooled fractions were concentrated by Amicon PM10 ultrafiltration.

Coupled Enzyme Assay. The enzymic activities of wild-type and mutant C-subunits were determined as described previously using a coupled enzyme spectophotometric assay (*28*). The oxidation of NADH, monitored spectrophotometrically as an absorbance decrease at 340 nm, was coupled to the production of ADP by lactate dehydrogenase and pyruvate kinase. C-Subunit (50−300 nM) was typically incubated in a 500 mL volume containing 50 mM Mops (pH 7.0), 5 mM ATP, 15 mM $MgCl_2$, 0.5 mM DTT, 1 mM phosphoenolpyruvate, 0.3 mM NADH, 12 units of lactate dehydrogenase, and 4 units of pyruvate kinase at 23 °C. Reaction mixtures were prepared in a disposable 1 mL cuvette, and reactions were initiated with varying amounts of Kemptide and monitored in a Hewlett-Packard 8453 spectrophotometer. Kemptide stock concentrations were determined by turnover with wild-type C-subunit under conditions of limiting peptide in the spectrophotometric assay. C-Subunit inhibitors were pre-equilibrated with enzyme in the assay mix for 1 min before addition of Kemptide during inhibition studies.

Radiochemical Assay. The enzyme (5−30 nM) was pre-equilibrated in assay mix containing 5 mM ATP, 15 mM $MgCl_2$, 0.5 mM DTT, 50 mM Mops (pH 7.0), and 10 mCi [γ-^{32}P]ATP for 5 min. Dilute stocks of wild-type or G55S C-subunit were prepared directly before each experiment with 0.5 mg/mL BSA. Kemptide was added to initiate a 10−30 min reaction in which the rate of phospho-Kemptide formation was linear with respect to time. The reaction (50 μL volume) was quenched with 20 mL of 50% acetic acid. Phospho-Kemptide was separated from unreacted ATP by a filter binding assay (*31*). A portion of each quenched reaction mixture (55 μL) was spotted onto a phosphocellulose filter disk and washed four times with 0.5% phosphoric acid. The filter disks were rinsed with acetone, dried, and counted on the ^{32}P channel in liquid scintillant. Control experiments quantitating the fraction of phospho-Kemptide retained on washed phosphocellulose disks were carried out as documented previously (*25*). Time-dependent formation of phospho-Kemptide was calculated by considering the total counts per minute (cpm) on each disk, the specific activity of the [γ-^{32}P]ATP label, the background phosphorylation, and the phospho=Kemptide retention on washed filter disks.

Measurement of Steady-State Kinetic and Inhibition Parameters. Steady-state kinetic rates for G50S and G55S were measured using the spectrophotometric assay, and those for G52S were measured using the radiochemical assay. For k_{cat} determinations, C-subunit concentrations were measured both by their spectrophotometric absorbance at 280 nm ($A_{0.1\%} = 1.2$) and by stoichiometric titration with known concentrations of a regulatory subunit type I mutant that is deficient in its ability to bind cAMP (*32*). Both methods yielded measurements that agreed within a factor of 2. k_{cat} was determined at saturating concentrations of ATP and Kemptide (5 mM each), and K_m values were determined at a saturating concentration of the fixed substrate.

Inhibition constants for three C-subunit inhibitors were measured to compare the ligand affinities between wild-type and mutant enzymes. AMPPNP, a nonhydrolyzable ATP analogue, and ADP are competitive inhibitors of wild-type C-subunit with respect to ATP and noncompetitive inhibitors with respect to Kemptide (*27*). The peptide LRRAALG is a competitive inhibitor of wild-type enzyme with respect to Kemptide and a noncompetitive inhibitor with respect to ATP (*33*). Apparent K_I values for AMPPNP, ADP, and LRRAALG were determined using Dixon plots and adjusted to their true values (*34*) using the concentration of the competing substrate.

Solution Viscosity Measurements. The relative viscosity (η^{rel}) of buffers containing sucrose was measured relative to 50 mM Mops at pH 7.0 and 23 °C using an Ostwald viscometer (*35*). Relative solvent viscosities of 1.0, 1.4, 1.7, 2.1, and 2.5 were obtained for buffers containing 0, 10, 18, 23, and 28% (w/v) sucrose, respectively. The measurements were made in triplicate and did not deviate by more than 2%.

Rapid Quench Flow Measurements. Pre-steady-state kinetic measurements were made using a KinTek Corp. Quench Flow Apparatus (model RGF-3). The apparatus contains three syringes driven by a stepping motor. Rapid quench flow experiments were executed by loading 1 mM enzyme, 50 mM Mops (pH 7.0), 11 mM magnesium chloride, and 1 mM ATP into one sample loop and 0.7−1.0 mM Kemptide into the other. Each reactant was pushed from a sample line into a reaction line by buffer driven from two of the syringes. Different combinations of reaction lines and stepping motor speeds were used to determine the reaction time (2−100 ms). The third syringe delivered 30% acetic acid that quenched the aged reaction as it exited the reaction line, and the mixture from this quenched reaction was collected in a 1.5 mL plastic vial. The amount of phospho-Kemptide was quantitated by the filter binding assay described above.

Data Analysis. Plots of initial velocity versus substrate were fit to the Michaelis−Menten equation (eq 1).

$$V_o = \frac{V_{max}[S]}{K_m + [S]} \quad (1)$$

Linear fits of Dixon plots were used to determine the K_I values for the competitive inhibitor of Kemptide, LRRAALG. Data from rapid quench flow time courses were fit to an empirical function containing a single exponential and a linear component

$$y = \alpha[1 - \exp(-k_b t)] + Lt \quad (2)$$

where y is the concentration of phospho-Kemptide, α is the observed "burst" amplitude, k_b is the observed single-exponential burst rate constant, and L is the observed linear rate. The data were fitted using the Macintosh computer graphics program Kaleidagraph (Synergy Software), which utilizes an iterative least-squares algorithm.

Molecular Modeling. Mutant structural models were generated using Insight and Discover (Biosym, 1995) on a

Table 1: Steady-State Kinetic Parameters for Wild-Type and Mutant C-Subunits[a]

	wild type	G50S	G52S	G55S
k_{cat} (s^{-1})	22 ± 2	9 ± 1 (1/2)	1.0 ± 0.5 (1/20)	7 ± 2 (1/3)
K_m(ATP) (μM)	20 ± 3	164 ± 16 (8)	256 ± 21 (12)	41 ± 5 (2)
k_{cat}/K_m(ATP) ($\mu M^{-1} s^{-1}$)	1.1 ± 0.2	0.055 ± 0.008 (1/20)	0.004 ± 0.001 (1/275)	0.17 ± 0.05 (1/6)
K_i(AMPPNP) (μM)	83 ± 10	423 ± 107 (5)	157 ± 6 (2)	88 ± 21 (1)
K_i(ADP) (μM)	8.7 ± 1.2	51 ± 6 (6)	8.0 ± 0.4 (1)	21 ± 3 (2)
K_m(Kemptide) (μM)	7.6 ± 1.8	326 ± 12 (50)	763 ± 114 (100)	121 ± 18 (17)
k_{cat}/K_m(Kemptide) ($\mu M^{-1} s^{-1}$)	2.9 ± 0.4	0.028 ± 0.006 (1/100)	0.001 ± 0.001 (1/3000)	0.058 ± 0.012 (1/50)
K_i(LRRAALG) (μM)	190 ± 20	2300 ± 500 (11)	2500 ± 100 (13)	1400 ± 100 (7)
K_m(LRRAALG)/K_m(Kemptide)	190/7.6	2300/326	2500/763	1400/120

[a] Values in parentheses represent the mutant/wild-type C-subunit ratio for a given parameter. k_{cat}/K_m is the apparent second-order association rate constant for low concentrations of ATP or Kemptide. K_i values are determined by Dixon plots.

Silicon Graphics Indigo workstation. First, the wild-type C-subunit−MnATP−IP_{20} ternary crystal structure (*36*) was energy minimized with relaxed amino acid side chains in vacuo. A steepest-decent, 5000-iteration minimization was employed using an AMBER (*37*) force field. Second, each NPL Gly was theoretically mutated to Ser. Third, each of the three mutated systems was energy minimized for 1000 iterations with (i) relaxed side chains, a fixed backbone, and a fixed MgATP level or (ii) relaxed side chains, a relaxed NPL backbone, and a fixed MgATP level. Crystallographic temperature factors (*B*-factors) were compared for C-subunit crystal structures solved for complexes with ATP (*36*) and without (*38*) ATP to determine the overall flexibility of the C-subunit. Temperature factors for amino acid backbones were calculated as an average of *B*-factors for four atoms, C_α, C_β, C, and N.

RESULTS

Steady-State Kinetic Analysis. Although the three glycines in the glycine-rich loop of the C-subunit were mutated previously to both Ala and Ser (*23*), only the Ser mutants were characterized in this study owing to partial solubility problems with some of the alanine mutants. With a comparison of the same substitution at each site, the results can be evaluated equivalently. The steady-state kinetic measurements for wild-type and mutant C-subunits, summarized in Table 1, are similar to those reported previously (*23*). Although mutations at Gly50 and Gly55 have small effects on k_{cat} (approximately 2-fold), substitution at Gly52 lowers turnover by more than 1 order of magnitude (12-fold). By comparison, G55S and G50S raise K_m(ATP) by 2- and 8-fold, respectively. All mutations affect K_m(Kemptide) but to varying extents (17−100-fold). The K_I values for AMPPNP and ADP were determined using Dixon plot analysis for wild-type and mutant C-subunits. While mutation at Gly52 has no effect on ADP affinity, G50S and G55S have K_I values that are raised 6- and 2-fold, respectively, relative to the wild-type value. Finally, the mutations affect equally the K_I values for the competitive inhibitor, LRRAALG, by approximately 10-fold.

Viscosometric Studies. Viscosometric experiments were performed to resolve individual steps in the enzyme reaction, in particular the rates of phosphoryl transfer and net product release. The data were interpreted according to a simple kinetic mechanism as shown in Scheme 1, where the phosphoryl transfer and net product release steps are designated by the rate constants k_3 and k_4 and the association and dissociation rate constants for the substrate are k_2 and k_{-2} at high ATP concentrations, respectively. Previous viscosometric studies with the wild-type C-subunit parametrized a phosphoryl transfer step, k_3, and a net product release step, k_4, from a linear plot of relative k_{cat} versus relative viscosity of the medium (*26*). The glycine mutants were analyzed in a similar fashion (Figure 2), where the relative k_{cat} is a ratio of this parameter measured in the absence and presence of various concentrations of the viscosogen, sucrose. Control experiments were performed to ensure that viscosogen concentrations used in this study perturbed k_{cat} only by altering the solvent viscosity and not the structure of the mutant C-subunits. Initial velocities for the mutants remained constant within 7% experimental error even after preincubation in 28% sucrose for 30 min at 23 °C.

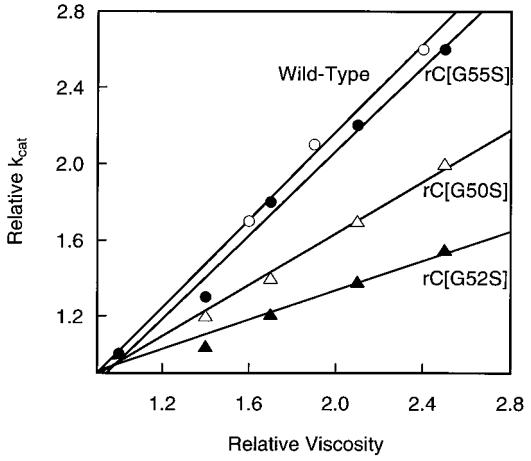

FIGURE 2: Microviscosometric analysis of wild-type (○), G50S (△), G52S (▲), and G55S (●) C-subunits. Relative k_{cat} is a ratio of the parameter measured in the absence and presence of viscosogen. Relative viscosities were determined as described in Experimental Procedures. Slopes from linear regressions of the data are reported in Table 2.

The slopes for each mutant C-subunit in Figure 2 are reported in Table 2 and accompanied by values of the individual rate constants, k_3 and k_4, derived from each slope according to the following equation:

$$(k_{cat})^{\eta} = \frac{k_3}{k_3 + k_4} \quad (3)$$

where $(k_{cat})^{\eta}$ is the slope of each linear plot in Figure 2. The wild-type values for k_3 and k_4 were measured previously (*25*). Since k_{cat} is maximally affected by viscosity [i.e., $(k_{cat})^{\eta} \approx 1$] for the wild-type enzyme, only a lower limit on k_3 can be

Table 2: Microviscosometric Perturbation of k_{cat} and Microscopic Rate Constants for Wild-Type and Mutant C-Subunits

	wild type	G50S	G52S	G55S
$(k_{cat})^{\eta}$	1.1 ± 0.1	0.7 ± 0.1	0.4 ± 0.1	1.1 ± 0.1
k_3 (s^{-1})	500 ± 60^a	29 ± 4 (17)	1.6 ± 0.5 (300)	75 ± 15^b (7)
k_4 (s^{-1})	20 ± 2	14 ± 2 (1.5)	2.5 ± 0.9 (8)	7 ± 2 (3)

[a] The microscopic rate constant for phosphoryl transfer, k_3, was determined previously in quench flow pre-steady-state studies (*25*). [b] k_3 is indirectly calculated for G55S from eq 4 since only a limit of ≥ 70 s^{-1} is extrapolated from $(k_{cat})^{\eta}$. Experimentally determined values for K_m(Kemptide), K_i(LRRAALG), and k_4 are used in the calculation of k_3.

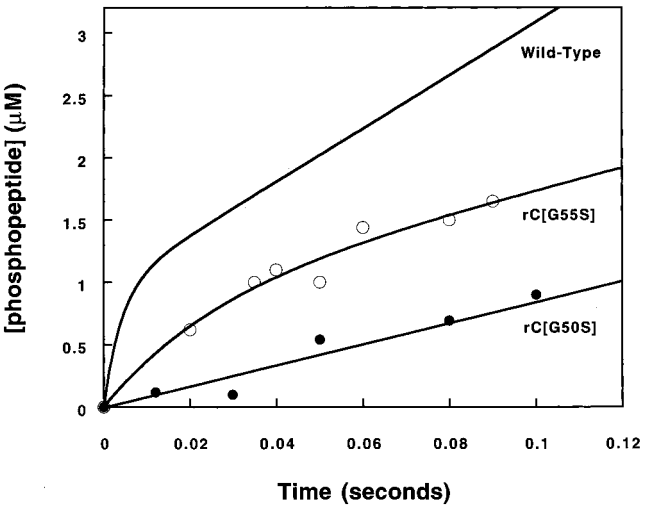

FIGURE 3: Pre-steady-state quench flow kinetic analysis of wild-type, G50S (●), and G55S (○) C-subunits. The experimental conditions for mutant C-subunits were 1 μM enzyme, 1 mM ATP, 11 mM magnesium chloride, 0.5 mM DTT, 50 mM Mops (pH 7.0), and 0.7−1.0 mM Kemptide. Wild-type C-subunit data are adapted from previous studies (*25*).

determined ($k_3 \geq 200$ s^{-1}). This is also true for G55S, where a lower limit is placed on k_3. In contrast, the partial viscosity effect on G50S and G52S permits exact measurements of k_3 and k_4. While only a lower limit can be placed on k_3 for G55S, we can estimate this value from the K_m and K_d for Kemptide assuming that the K_I for LRRAALG is a good measure of the substrate affinity. If the substrate is in rapid exchange with the enzyme, k_3 can be evaluated from K_m and K_d using Scheme 1 [i.e., $K_m = K_d k_4/(k_3 + k_4)$]. This analysis predicts that the rate of phosphoryl transfer in G55S is 75 s^{-1}, a value consistent with the lower limit in Table 2.

Pre-Steady-State Kinetic Analyses. G50S and G55S were also analyzed in pre-steady-state rapid quench flow experiments, which directly measure phosphoryl transfer rates. In this experiment, C-subunit (1 μM), ATP (1 mM), and $MgCl_2$ (11 mM) in 50 mM Mops (pH 7.0) were mixed with Kemptide in concentrations equal to approximately $^1/_2K_I$ (LRRAALG) (i.e., 1 mM for G50S and 0.7 mM for G55S). Control experiments, in which the reaction was quenched immediately with a 30% acetic acid/Kemptide mixture, determined both background activity (15%) and quenching efficiency (95%). Time-dependent traces of product formation for both mutants along with that of the wild-type enzyme are displayed in Figure 3. For comparison, the pre-steady-state kinetic trace for wild-type cAPK is shown. The data were fitted to eq 2 for G55S and a linear function for G50S. Values of 30 ± 10 s^{-1}, 0.90 ± 0.17 μM, and 8 ± 3 s^{-1} were obtained for k_b, α, and L/[E], respectively, for G55S. For G50S, a linear rate constant of 7 ± 1 s^{-1} was obtained. The burst rate constant for G55S is 50% lower than the predicted value for the phosphoryl transfer rate on the basis of viscosity measurements and a consideration of the inhibitor binding constant (Table 1). However, the burst rate for G55S is an observed value that reflects not only the rate of phosphoryl transfer but also the affinity of the substrate. It was shown previously that, when the substrate is in rapid exchange, the burst rate constant can be related to the substrate concentration by eq 4

$$k_b = \frac{k_3[S]}{K_d + [S]} + k_4 \quad (4)$$

When the values for K_d (K_I for LRRAALG), [S] (0.7 mM), and k_4 (7 s^{-1}) are inserted, the burst rate constant can be used to measure k_3. This calculated value, 70 s^{-1}, is similar to the estimate derived from the viscosity measurements.

Molecular Models and Backbone Flexibility. Structural models were generated for each mutant to assess motion in the NPL as a consequence of the Gly to Ser mutations. Panels a−c of Figure 4 depict structural models energy minimized with rigid (red) and relaxed (blue) backbones. The G50S Ser effects an NPL conformational change (Figure 4a) so the nucleotide ribose can be accommodated. The G52S Ser swings inward (Figure 4b) to avoid unfavorable van der Waals repulsion with the nucleotide γ-phosphate, thereby causing backbone torsion ($\Delta\phi = 100°$, $\Delta\Psi = 20°$) and displacement of the NPL backbone (0.8 Å). Errors calculated for the ternary complex crystallographic model do not exceed 0.5 Å on the basis of an *R*-factor of 0.21 and a resolution of 2.2 Å. The G55S Ser does not effect significant conformational changes (Figure 4c). Figure 4d compares crystallographic *B*-factors from structures with and without ATP. While Gly52 and Ser53 are highly flexible in the binary complex that lacks ATP, these amino acids are ordered in the ternary complex when both ATP and the inhibitor peptide are present (*14*).

DISCUSSION

The glycine-rich loop in protein kinases is a characteristic feature of the enzyme active site, and interactions between amino acids in this loop and bound nucleotide appear to be crucial for protein kinase function on the basis of the available C-subunit crystal structures (*14*, *20*, *21*). Although perturbations in steady-state kinetic parameters were measured previously for mutations of the C-subunit of cAPK (*23*) that were specifically perturbed at the three glycines in the glycine-rich loop, effects on substrate binding, phosphoryl transfer, and net product release were not determined. Each Gly in the glycine-rich loop of the cAPK C-subunit was mutated to Ser. The mutant proteins were purified to homogeneity and then subjected to steady-state and pre-steady-state kinetic analyses so that the real contribution of each amino acid in the loop on individual enzymatic steps could be assessed. The mutant kinetic parameters are compared to the complete kinetic mechanism established for the wild-type C-subunit. This mechanism, summarized in Scheme 1, was derived from the application of rapid quench flow and viscosometric studies on the phosphorylation of Kemptide (*25*).

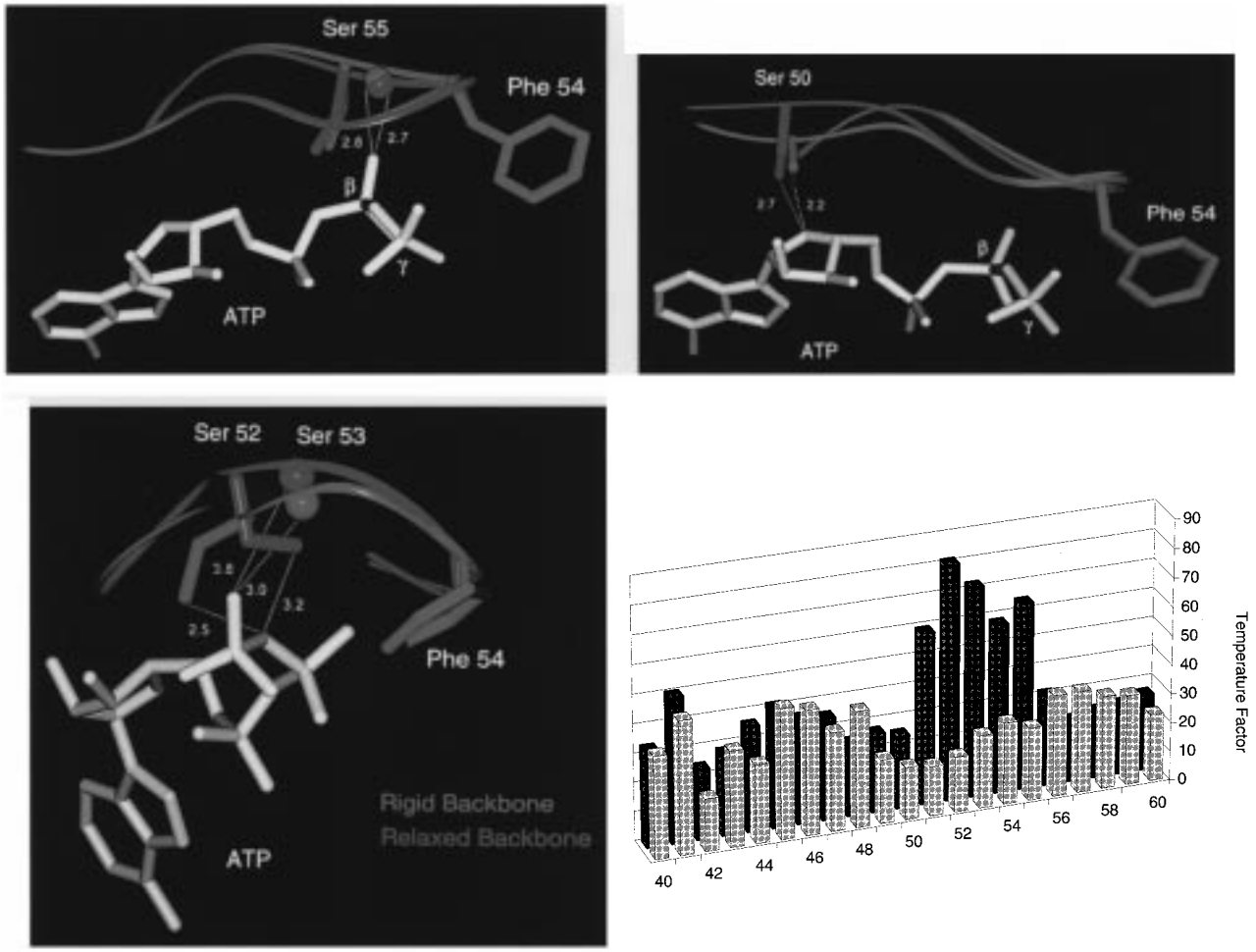

FIGURE 4: Molecular modeling studies for wild-type and mutant C-subunits. A structural model for each mutant (a, top left; b, top right; and c, bottom left) is shown with the backbone in rigid (red) and relaxed (blue) conformations. Panel c depicts the nucleotide γ-phosphate pointing at the reader. Averaged crystallographic temperature factors (*B*-factors) for amino acids 40−60 (d, bottom right) are compared for C-subunit structures of the ternary complex with ATP and PKI(5−24) (light gray) and the binary complex with only PKI(5−24) (dark gray).

Effects of Mutation on Ligand Affinity. Mutations at all glycine positions in the glycine-rich loops of cAPK result in decreases in the apparent affinity of ATP and Kemptide (Table 1). While the results of these apparent effects have a profound and direct influence on the catalytic efficiency of the mutant enzymes relative to that of the wild type (*23*), comparisons of the steady-state kinetic parameters are not good indicators of the true effects on ligand affinity. The fast rate of phosphoryl transfer makes it difficult to obtain K_d measurements for ATP or Kemptide directly. For the wild-type enzyme, the K_m(ATP) is the ratio of the net product release step (k_4) and the association rate constant (k_1) (*26*). The K_m is only coincidentally similar to the measured K_d for ATP. However, since all mutations in this study have raised K_m(ATP) values and reduced values for k_3 and k_4 (Table 2), we presume that this apparent affinity parameter now reflects the true affinity so that K_m and K_d can be used interchangeably for ATP. The K_m for Kemptide is lower than the true K_d by the factor $k_4/(k_3 + k_4)$ when the substrate is in rapid exchange with the enzyme (*25*). Since k_3 is still comparable or even larger than k_4 for all mutations, K_m-(Kemptide) does not reflect the true affinity and must be analyzed carefully.

To obtain the effects of each mutation on ligand affinity without the complication of kinetic perturbations, we measured the dissociation constant for several competitive inhibitors of cAPK (Table 1). For nucleotide binding effects, the K_I values of two competitive inhibitors, ADP and AMPPNP, were measured (Table 1) for the wild-type and mutant proteins. All three mutations have a modest or no effect on the affinity of AMPPNP with K_I values raised between 1- and 5-fold relative to that of the wild type. These effects are consistent with the elevations in K_m for ATP with the exception of G52S, where the comparative changes in the K_m for ATP and the K_I for AMPPNP differ by 6-fold. We will discuss the potential significance of this variance later. Only G50S affects the affinity of ADP (5-fold). Moreover, the data indicate that mutations in the conserved glycines in the NPL have small effects on nucleotide affinity. G52S and G55S bind AMPPNP and ADP with affinities similar to those for wild-type C-subunit, while G50S has an about 5-fold effect on both ligands. Using the comparisons of these inhibition constants, we conclude that Gly50 is the only glycine in the NPL that is important for nucleotide affinity.

The true affinity of Kemptide was measured using the competitive inhibitor ala-Kemptide. Previous studies have shown that the K_I for this peptide is a true measure of Kemptide affinity in the active site of the wild-type enzyme (*25*) and is, therefore, likely to reflcet directly the affinity

of the substrate for the mutant enzymes. Mutation at each glycine in the NPL equally affected the affinity of ala-Kemptide by 7−13-fold relative to that of the wild type (Table 1). This effect is surprising since the NPL glycines do not contact directly the substrate, implying that the mutations affect other residues that make contact with the substrate. These long-range effects imply that the glycine-rich loop, although not directly contacting Kemptide, positions the substrate in the active site.

Effects of Mutation on Phosphoryl Transfer. Viscosometric and pre-steady-state kinetic methods were used to determine the effects of glycine replacement on phosphoryl transfer. Viscosometric analyses of wild-type cAPK indicate that phosphoryl transfer is, at least, 10-fold faster than maximum turnover (*26*). The application of rapid quench flow analyses placed the rate constant for phosphoryl transfer at 500 s^{-1}, approximately 25-fold higher than the net release rate for products (*25*). Partial viscosity effects on k_{cat} were measured for G50S and G52S, allowing estimates of k_3 to be made (Table 2). Since a full viscosity effect was measured for G55S, a direct measurement of the phosphoryl transfer rate constant was not possible, although a consideration of the dissociation constant for the substrate (i.e., K_I for LRRAALG) was used to estimate k_3 (Table 2). Rapid quench flow analyses of G55S and G50S were also used to evaluate k_3. The corrected burst rate constant for G55S is 70 s^{-1}, a value consistent with the estimates from viscosity measurements. No burst phase was observed for G50S since the dissociation constant for the substrate is high ($K_I = 2.3$ mM) and the rate of phosphoryl transfer is similar to the net rate for product release (Table 2). The linear rate for G50S is close to the steady-state rate under conditions of nonsaturating Kemptide. The results indicate that all three mutations have effects on the rate of phosphoryl transfer that generally were equivalent to or larger than the effects on nucleotide affinity. The most pronounced effect was observed for replacement of Gly52, where the rate of phosphoryl transfer was lowered 300-fold relative to that of the wild type (Table 2). Surprisingly, Gly52 plays the most significant role in controlling catalysis, although it does not directly contact the phosphates of ATP.

Although Gly52 does not make direct contact with the nucleotide, it may position the neighboring Ser side chain (Ser53) which makes a direct contact with the γ-phosphate of ATP. The structural model in Figure 4b suggests that this hydrogen bond can no longer form in G52S as the distance between the Ser53 amide nitrogen and the ATP oxygen increases from 3.0 to 3.8 Å. This hydrogen bond may stabilize the transition state by positioning the γ-phosphate for nucleophilic addition of the hydroxyl acceptor and delocalizing electron density that may develop in the transition state.

Effects of Mutation on Net Product Release. The viscosity measurements provide an estimate for the net rate of product release which may be limited by the release of ADP or phosphopeptide, one or more conformational changes, or a combination of all these events. While G50S has no measurable influence on these events, G52S and G55S reduce net product release by 8- and 3-fold, respectively. Recently, a catalytic trapping experiment was implemented that directly measured the dissociation rate constant for ADP using rapid quench flow analyses (*22*). These studies showed that the rate Kemptide turnover is close to the dissociation rate constant for ADP. For wild-type cAPK, this means that the measure of k_{cat} is a direct measure of the dissociation rate constant for ADP. If there is no change in the rate-determining step for net product release upon mutation, both G52S and G55S must improve the affinity of ADP. However, no reductions in ADP affinity were found. In fact, the K_I for ADP is raised 6- and 2-fold for G50S and G55S, respectively, although k_4 is reduced 1.5- and 3-fold, respectively (Table 1). While it is possible that these discrepancies may be explained by altered association rate constants for ADP and the mutants, we propose that these inconsistencies arise from changes in the rate-determining step for turnover owing to the participation of conformational changes. While it is difficult to define the nature of these conformational changes, the molecular model presented in Figure 4b hints at a possible structural change in the glycine-rich loop that could explain the lower k_4 for G52S. The introduction of a Ser side chain as well as the torsion in backbone dihedral angles (Figure 4b) may decrease the flexibility of the loop in G52S. ADP release may require the flexibility inherent to the NPL, and increased NPL rigidity in G52S could cause a decreased product release rate constant.

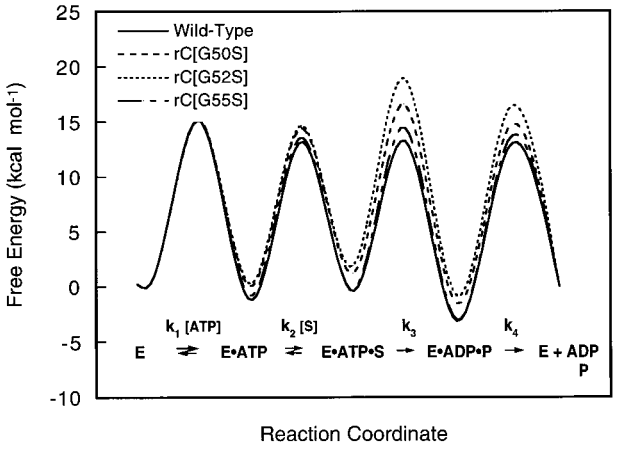

FIGURE 5: Reaction pathway free energy diagrams for wild-type and mutant C-subunits. Transition-state energies were calculated by applying the Eyring equation to rate constants parametrized in this and other studies (*26*). The free enzyme ground state was arbitrarily set to zero for each C-subunit, and subsequent ground-state free energies were calculated from equilibrium constants for steps along the reaction pathway. The internal equilibrium constant, determining the relation between ground-state energies for the substrate and product complexes, is assumed not to change upon mutation.

Conservation of NPL Glycines. A free energy diagram assembled for the wild type, G50S, G52S, and G55S (Figure 5) summarizes the perturbations in kinetic parameters caused by these mutations. Transition-state energies were calculated by applying the Eyring equation to rate constants parametrized in this and other studies (*26*). Relative perturbations in ground-state free energies were calculated from equilibrium constants for steps along the reaction pathway. Assumptions included in the free energy diagrams are as follows: (i) mutations do not perturb free enzyme ground-state free energies, (ii) mutations do not perturb association microscopic rate constants (*39*), and (iii) the internal equilibrium constant, determining the relationship between substrate and product ternary complex ground-state free energies, is not perturbed for the mutant enzymes.

Glycines are stringently conserved in NPLs because their lack of a side chain minimizes van der Waals repulsion between the NPL and nucleotide while maximizing backbone flexibility. Glycine-enhanced flexibility may facilitate enzyme−ligand interactions in such dynamic processes as induced-fit substrate binding and conformational-linked product release. In the midst of these dynamic processes, glycine's lack of steric volume permits interactions, such as hydrogen bonds formed between the NPL backbone and nucleotide, that stabilize the transition state. The minimal steric repulsion inherent to glycine allows the protein kinase NPL to (i) position the nucleotide ribose (Figure 4a) and γ-phosphate (Figure 4b) preceding catalysis, (ii) form a transition-state stabilizing hydrogen bond between its backbone and a γ-phosphate oxygen during catalysis (Figure 1), and (iii) maximize flexibility (Figure 4d) during a conformational switch that may be partially responsible for rate-limiting nucleotide diphosphate release after catalysis.

ACKNOWLEDGMENT

We appreciate Dr. John Lew's and Dr. Sarah Cox's insights that impacted the paper's content.

REFERENCES

1. Hescheler, J., Klienz, F.-J., Schultz, G., and Wittinghofer, A. (1991) *Cell 3*, 127−133.
2. Bossemeyer, D. (1994) *Trends Biochem. Sci. 19*, 201−205.
3. Rossmann, M. G., Moras, D., and Olsen, K. W. (1974) *Nature 250*, 194−199.
4. Bennett, W. S., and Huber, R. (1984) *CRC Crit. Rev. Biochem. 15*, 291−384.
5. Filman, D. J., Bolin, J. T., Matthews, D. A., and Kraut, J. (1982) *J. Biol. Chem. 257*, 13663−13672.
6. Krengel, U., Schlichting, I., Scherer, A., Schumann, R., Frech, M., John, J., Kabsch, W., Pai, E. F., and Wittinghofer, A. (1990) *Cell 62*, 539−548.
7. Muller, C. W., and Schulz, G. E. (1992) *J. Mol. Biol. 224*, 159−177.
8. Story, R. M., and Steitz, T. A. (1992) *Nature 355*, 374−376.
9. Berchtold, H., Reshetnikova, L., Reiser, C. O., Schirmer, N. K., Sprinzl, M., and Hilgenfeld, R. (1993) *Nature 365*, 126−132.
10. Saraste, M., Sibbald, P. R., and Wittinghofer, A. (1990) *Trends Biochem. Sci. 15*, 430−434.
11. De Bondt, H. L., Rosenblatt, J., Jancarik, J., Jones, H. D., Morgan, D. O., and Kim, S. H. (1993) *Nature 363*, 595−602.
12. Hu, S.-H., Parker, M. W., Lei, J. Y., Wilce, M. C. J., Benian, G. M., and Kemp, B. E. (1994) *Nature 369*, 578−581.
13. Hubbard, S. R., Wei, L., Ellis, L., and Hendrickson, W. A. (1994) *Nature 372*, 746−754.
14. Narayana, N., Cox, S., Shaltiel, S., Taylor, S. S., and Xuong, N. (1997) *Biochemistry 36*, 4438−4448.
15. Zhang, F., Strand, A., Robbins, D., Cobb, M. H., and Goldsmith, E. J. (1994) *Nature 367*, 704−711.
16. Hanks, S. K., and Hunter, T. (1995) *FASEB J. 9*, 576−596.
17. Zetterqvist, Ö. Z., Ragnarsson, U., and Engstrom, L. (1990) *Peptides and Protein Phosphorylation*, CRC Press, Inc., Boca Raton, FL.
18. Cook, S. J., and McCormick, F. (1993) *Science 262*, 1069−1072.
19. Krebs, E. G., Graves, D. J., and Fischer, E. H. (1959) *J. Biol. Chem. 234*, 2867−2873.
20. Zheng, J., Knighton, D. R., Ten Eyck, L. F., Karlsson, R., Xuong, N.-h., Taylor, S. S., and Sowadski, J. M. (1993) *Biochemistry 32*, 2154−2161.
21. Bossemeyer, D., Engh, R. A., Kinzel, V., Ponstingl, H., and Huber, R. (1993) *EMBO J. 12*, 849−859.
22. Zhou, J., and Adams, J. (1997) *Biochemistry 36*, 2977−2984.
23. Hemmer, W., McGlone, M. L., and Taylor, S. S. (1997) *J. Biol. Chem. 272*, 16946−16954.
24. Lee, J.-h., Maeda, S., Angelos, K. L., Kamita, S. G., Ramachandran, C., and Walsh, D. A. (1992) *Biochemistry 31*, 10616−10625.
25. Grant, B. D., and Adams, J. A. (1996) *Biochemistry 35*, 2022−2029.
26. Adams, J. A., and Taylor, S. S. (1992) *Biochemistry 31*, 8516−8522.
27. Whitehouse, S., and Walsh, D. A. (1983) *J. Biol. Chem. 258*, 3682−3692.
28. Cook, P. F., Neville, M. E., Vrana, K. E., Hartl, F. T., and Roskoski, R. (1982) *Biochemistry 21*, 5794−5799.
29. Herberg, F. W., Bell, S. M., and Taylor, S. S. (1993) *Protein Eng. 6*, 771−777.
30. Hemmer, W., McGlone, M. M., and Taylor, S. S. (1997) *Anal. Biochem. 245*, 115−122.
31. Kemp, B. E., Graves, D. J., Benjamini, E., and Krebs, E. G. (1977) *J. Biol. Chem. 252*, 4888−4894.
32. Neitzel, J. J., Dostmann, W. R. G., and Taylor, S. S. (1991) *Biochemistry 30*, 733−739.
33. Yoon, M.-Y., and Cook, P. F. (1987) *Biochemistry 26*, 4118−4125.
34. Segel, I. H. (1975) *Enzyme Kinetics*, John Wiley & Sons, New York.
35. Shoemaker, D. P., and Garland, C. W. (1962) *Experiments in Physical Chemistry*, 2nd ed., McGraw-Hill, New York.
36. Zheng, J., Trafny, E. A., Knighton, D. R., Xuong, N.-h., Taylor, S. S., Ten Eyck, L. F., and Sowadski, J. M. (1993) *Acta Crystallogr. D49*, 362−365.
37. Weiner, S. J., Kollman, P. A., Case, D., Singh, U. C., Ghio, C., Alagona, G., Profeta, S. J., and Weiner, P. (1984) *J. Am. Chem. Soc. 106*, 765−784.
38. Knighton, D. R., Bell, S. M., Zheng, J., Ten Eyck, L. F., Xuong, N.-h., Taylor, S. S., and Sowadski, J. M. (1993) *Acta Crystallogr. D49*, 357−361.
39. Adams, J. A., and Taylor, S. S. (1993) *Protein Sci. 2*, 2177−2186.

BI972987W